Geochemical Perspectives Letters

Large Cu endowment in the Tibetan Plateau as a result of dual stage mantle fertilisation

X. Wang[1,2], L. Gao[1,3], Z. Bai[1], M. Huang[1], J. Zhu[1*], R. Yin[1*]

https://doi.org/10.7185/geochemlet.2519

Abstract

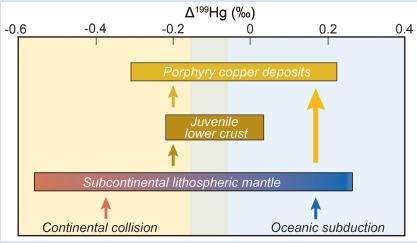

The Himalayan-Tibetan orogenic belt hosts numerous world class porphyry copper deposits (PCDs), whose metal sources are controversial. Mercury isotopes display mass independent fractionation during photoreactions, producing positive Δ^{199}Hg in marine sediments and negative Δ^{199}Hg in terrestrial sediments. Here, we observe non-zero Δ^{199}Hg (−0.29 to +0.21 ‰) in PCDs from the Himalayan-Tibetan orogenic belt. These values do not support the sole contribution of Hg from juvenile lower crustal rocks, which contain terrestrially derived Hg and display negative Δ^{199}Hg (−0.20 to +0.01 ‰). The subcontinental lithospheric mantle (SCLM) with highly variable Δ^{199}Hg (−0.54 to +0.25 ‰) can be another Hg source for PCDs. The positive and negative Δ^{199}Hg values observed in PCDs and the SCLM suggest the contribution of Hg from both marine and terrestrial sediments. As the Himalayan-Tibetan orogenic belt underwent Neo-Tethys oceanic subduction followed by Indian-Eurasia continental collision, dual stage fertilisation of the SCLM *via* oceanic subduction and continental collision likely played an essential role in the generation of metal- and volatile-rich magmas and the associated large number of PCDs. This study offers key insights into the metal source of PCDs in the Himalayan-Tibetan orogenic belt.

Received 15 February 2025 | Accepted 6 May 2025 | Published 10 June 2025

Introduction

Porphyry copper (Cu) deposits (PCDs) provide ~75 % of the global Cu resources. Oceanic subduction and continental collision trigger the large metallogeny of PCDs at convergent plate boundaries. PCDs related to Pacific plate subduction typically occur in the Circum-Pacific belt, particularly in the Andes, Papua New Guinea, and the Philippines (Sillitoe, 2010; Wilkinson, 2013). PCDs related to collision of the African, Arabian and Indian Plates with the Eurasian Plate occur in the Alpine-Himalayan belt (Richards, 2009). PCDs in these two belts provide a window to probe plate subduction and associated effects on large Cu endowments. A variety of geochemical tools (*e.g.*, Sr, Nd, Pb and Cu isotopes) have been employed to constrain the sources of metals in PCDs of the Alpine-Himalayan belt, but it remains debated whether the ore-forming metals are sourced from the partial melting of sulfide-rich juvenile lower crustal rocks (Li *et al.*, 2011; Hou *et al.*, 2020) or the fertile subcontinental lithospheric mantle (SCLM) (Xu *et al.*, 2016; Zheng *et al.*, 2019).

Mercury (Hg) is a chalcophile metal and an important component in PCDs (Xu *et al.*, 2024). The seven natural stable isotopes of Hg (^{196}Hg, ^{198}Hg, ^{199}Hg, ^{200}Hg, ^{201}Hg, ^{202}Hg, ^{204}Hg) display mass-dependent fractionation (Hg-MDF, reported as δ^{202}Hg) and mass-independent fractionation (Hg-MIF, reported as Δ^{199}Hg). Hg-MDF occurs during various geochemical processes (*e.g.*, microbial Hg(II) reduction, Hg(II) methylation, Hg(0) volatilisation), whereas Hg-MIF occurs mainly during photochemical reactions (Blum *et al.*, 2014). The primitive mantle displays near-zero Δ^{199}Hg values (0.00 ± 0.10 ‰; 2 s.d.; Moynier *et al.*, 2021). In contrast to magmatic Hg isotope signatures, Hg(II) photoreduction results in negative Δ^{199}Hg signals in terrestrial systems (−0.6 to 0 ‰; soil and vegetation) and positive Δ^{199}Hg values in marine systems (0 to +0.3 ‰; sediments and seawater) (Blum *et al.*, 2014). The distinctive Δ^{199}Hg signatures of terrestrial, marine and mantle reservoirs allow for tracing the source of metals in magmatic and hydrothermal systems (Yin *et al.*, 2024). Positive Δ^{199}Hg values have been observed in arc basalts and hydrothermal systems (0 to +0.3 ‰; epithermal Au deposits and porphyry Mo deposits) in the Circum-Pacific belt, reflecting large scale recycling of metals from marine reservoirs *via* oceanic subduction (Deng *et al.*, 2021; Yin *et al.*, 2022; Gao *et al.*, 2024a).

A recent study observed highly variable Δ^{199}Hg in fertile porphyry-related magmas (−0.30 to +0.22 ‰) and coeval ultrapotassic mafic rocks (−0.54 to +0.25 ‰) in the Himalayan-Tibetan orogenic belt, highlighting that PCDs receive metals or volatiles from the SCLM modified by subducted materials (Xu *et al.*, 2024). However, there are yet undefined Hg isotopic reservoirs related to PCDs, including lower crustal rocks and the ore-forming sulfides. In this work, we investigate the Hg isotopic composition of these reservoirs in the Himalayan-Tibetan orogenic belt to gain an understanding of the metal sources of PCDs.

1. State Key Laboratory for Critical Mineral Research and Exploration, Institute of Geochemistry, Chinese Academy of Sciences, Guiyang 550081, China
2. University of Chinese Academy of Sciences, Beijing 100049, China
3. College of Earth Sciences, Jilin University, Changchun 130061, China
* Corresponding authors (emails: R. Yin, yinrunsheng@mail.gyig.ac.cn; J. Zhu, zhujingjing@mail.gyig.ac.cn)

Geological Background

The eastern part of the Alpine-Himalayan orogenic belt comprises a series of blocks and micro-continents (Fig. 1a). Subduction of the Palaeo-Tethys Ocean in the Palaeozoic caused collision of these blocks and micro-continents (Metcalfe, 2021). The Neo-Tethys Ocean was closed in the Late Cretaceous, followed by the collision of the Indian and Eurasian continents (Metcalfe, 2021). The Songpan-Ganzi, Qiangtang, Lhasa and Himalaya Terranes, divided by the Jinsha, Bangong-Nujiang and Yarlung-Zangbo suture zones, mark the sequential closure of the Palaeo-, Meso- and Neo-Tethys oceans, respectively (Zheng *et al.*, 2021). The Tibetan Plateau hosts the Yulong and the Gangdese porphyry Cu belts, which contain numerous world-class PCDs formed during the Indian-Eurasian collisional orogeny.

The Yulong porphyry Cu belt (Fig. 1b) follows the northwestward trend of the Red River-Ailao Shan Fault, *i.e.* a sinistral fault system that emerged due to the Indian-Eurasian continental collision. It comprises Proterozoic to early Palaeozoic crystalline folded basement and middle to late Palaeozoic carbonate and clastic sedimentary rocks, and distributes >20 PCDs (*e.g.*, Yulong) with mineralisation ages (~40 Ma) synchronous with nearby Eocene alkaline magmatism (Yang and Cooke, 2019). Ore-bearing porphyries at Yulong are mainly monzonite granite porphyries containing assemblages of pyrite, chalcopyrite and molybdenite (Fig. S-1). The Yulong PCD is associated with potassic, sericitic, and epidote alterations,

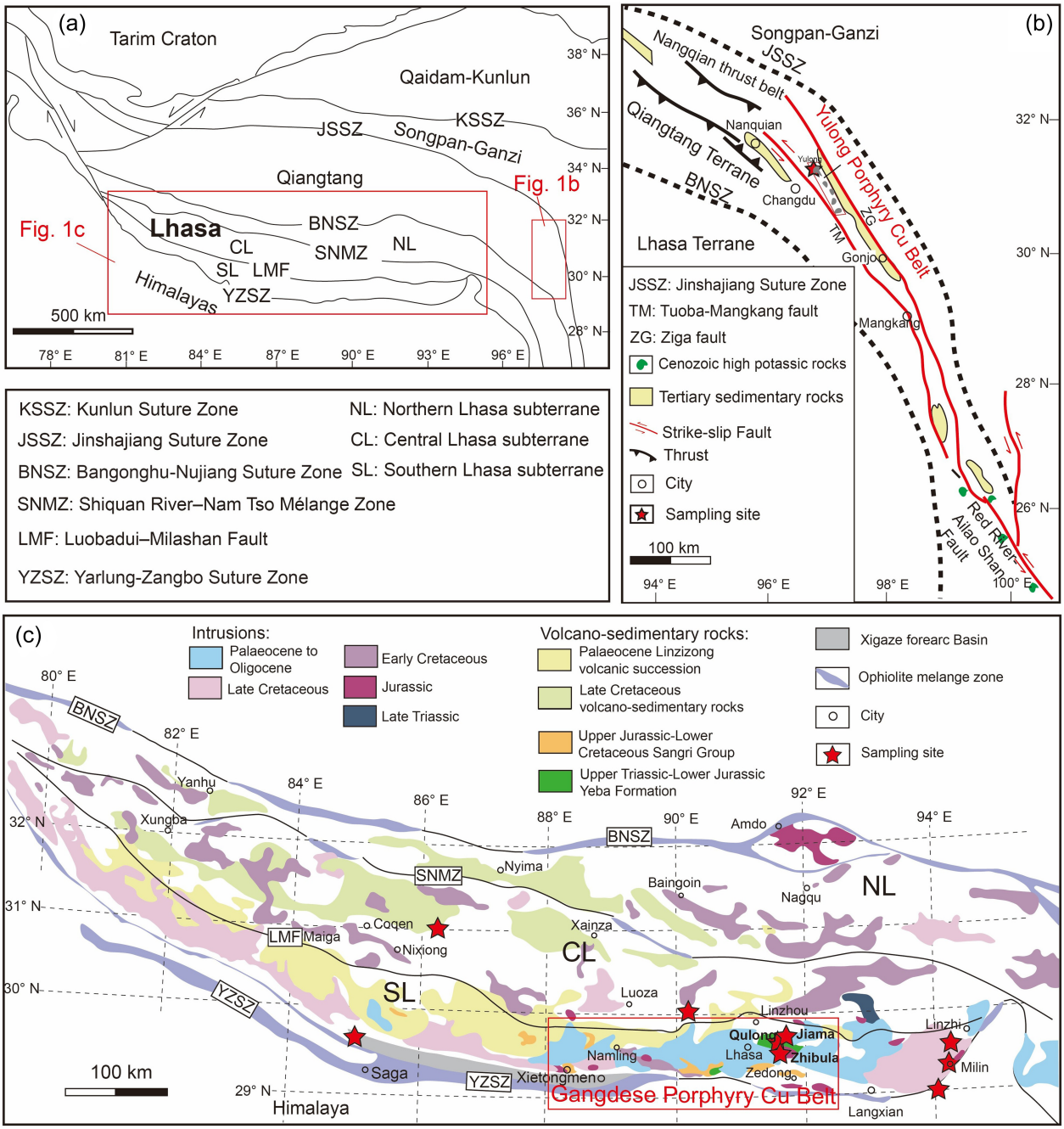

Figure 1 Geological map showing **(a)** the Himalayan-Tibetan orogen, **(b)** the Yulong porphyry Cu belt (after Liang *et al.*, 2006) and **(c)** the Gangdese porphyry Cu belt (after Sun *et al.*, 2024).

manifested as the widespread distribution of quartz-biotite veins, secondary K-feldspar, and epidote-altered zones, accompanied by localised development of sulfide mineralisation (Fig. S-2).

The Gangdese porphyry Cu belt is located in the Lhasa terrane (Fig. 1c), which is a microcontinental fragment comprising Precambrian basement rocks, Palaeozoic to Mesozoic sedimentary formations, and Mesozoic to Cenozoic igneous rocks (Sun *et al.*, 2024). This belt was formed during post-collision between the Indian and Eurasian continents and hosts abundant Miocene ultrapotassic magmatic rocks and numerous PCDs (*e.g.*, Jiama, Qulong, and Zhibula) with mineralisation ages of 16 to 14 Ma (Hou *et al.*, 2011). Mineralised intrusions in the Gangdese PCDs are mainly monzonite granite and quartz monzonite porphyries, containing assemblages of pyrite, chalcopyrite, molybdenite, magnetite and bornite (Fig. S-3). The deposits are characterised by pyrite-sericitisation alteration in Qulong, sericitic and skarn-related alteration in Jiama, and epidote-garnet alteration in Zhibula (Fig. S-4).

Methods

A total of 43 sulfide-bearing bulk ore samples (*i.e.* mineralised porphyries) were collected from the Yulong, Qulong, Jiama, and Zhibula deposits. Sulfides (pyrite, $n = 26$; chalcopyrite, $n = 16$; bornite, $n = 4$) were separated from the bulk ore samples. Sulfides were pre-concentrated using flotation with xanthate as the collector, followed by hand picking under a binocular microscope to ensure high purity. Magmatic rocks ($n = 19$) representing the juvenile lower crust and ultrapotassic mafic rocks ($n = 5$) representing the SCLM from the Gangdese area were also collected. Detailed information for the samples can be found in Supplementary Tables S-1 and S-2. All the samples were prewashed with 18.2 MΩ cm water, air dried, ground to a particle size of 200 mesh, and homogenised in an agate mortar for petrochemical analysis.

The major elements of rock powders were analysed using X-ray fluorescence (XRF) spectrometry at ALS Guangzhou with a PANalytical PW5400 instrument, which yielded an analytical uncertainty of <5 % for sample duplicates. The loss on ignition (LOI) was measured according to the percentage weight loss before and after heating the samples at 1000 °C in a muffle furnace. LOI values of all samples are <3 wt. % (Table S-3), indicating limited alteration effects. The major element concentrations of the lower crustal rocks ($n = 19$) have been recently reported (Sun *et al.*, 2024).

Total Hg (THg) concentrations and Hg isotopic compositions were determined at the Institute of Geochemistry, Chinese Academy of Sciences. Concentrations of THg were directly measured using a Lumex R915+ Hg analyser (detection limit 50 pg Hg), which yielded Hg recoveries of 90–110 % ($n = 8$) for GSS-4 standard reference material and uncertainties of <10 % (2 s.d.) for sample duplicates. Based on the measured THg concentrations, variable amounts of sample powders containing 10 ng Hg were weighed and prepared using a two stage combustion furnace for preconcentrating Hg into 5 mL of 40 % acid mixture (HNO_3/HCl = 2/1, v/v), following previous methods (Zerkle *et al.*, 2020; Gao *et al.*, 2024b). The Hg blank of the acid mixture is below 0.05 ng/mL. Preparation of zero sample powders yielded a method blank of less than 50 pg Hg in the sample solution. Pretreatment of standard reference material (GSS-4, soil) yielded Hg recoveries of 90–110 % ($n = 8$). The Hg preconcentrated solutions were diluted to 1 ng/mL with 10–20 % of acid mixture (HNO_3/HCl = 2/1, v/v) before Hg isotopic analysis at the Institute of Geochemistry, Chinese Academy of Sciences, using a Thermo Scientific Neptune Plus multi-collector inductively coupled plasma mass spectrometry (Supplementary Text S-1; Yin *et al.*, 2016). Hg-MDF is expressed as δ^{202}Hg in ‰ in reference to the NIST-3133 Hg standard:

$$\delta^{202}\mathrm{Hg}(‰) = [(^{202}\mathrm{Hg}/^{198}\mathrm{Hg}_{\mathrm{sample}})/(^{202}\mathrm{Hg}/^{198}\mathrm{Hg}_{\mathrm{standard}}) - 1] \times 1000 \quad \text{Eq. 1}$$

MIF is reported in Δ notation as the difference between the measured δ^{xxx}Hg values and theoretically predicted values:

$$\Delta^{xxx}\mathrm{Hg} = \delta^{xxx}\mathrm{Hg} - \delta^{202}\mathrm{Hg} \times \beta \quad \text{Eq. 2}$$

where *xxx* represents 199, 200, or 201, and β is 0.252 for ^{199}Hg, 0.5024 for ^{200}Hg, and 0.752 for ^{201}Hg (Blum and Bergquist, 2007). NIST-3177 secondary standard solutions were measured every 10 samples. The overall average and uncertainty of NIST-3177 (δ^{202}Hg = −0.53 ± 0.06 ‰, Δ^{199}Hg = −0.02 ± 0.04 ‰; Δ^{200}Hg = +0.01 ± 0.03 ‰; Δ^{201}Hg = −0.02 ± 0.06 ‰; 2 s.d., n = 10) and GSS-4 (δ^{202}Hg = −1.69 ± 0.13 ‰; Δ^{199}Hg = −0.41 ± 0.06 ‰; Δ^{200}Hg = −0.02 ± 0.06 ‰; Δ^{201}Hg = −0.37 ± 0.06 ‰; 2 s.d., $n = 8$) agree well with previous results (Table S-4; Blum and Berquist, 2007; Deng *et al.*, 2021; Gao *et al.*, 2024b). The larger values of standard deviation (2 s.d.) for either NIST-3177 or GSS-4 are used to reflect analytical uncertainties.

Results

As shown in Tables S-1 and S-2 and Figure 2a, the studied sulfide samples show large variations in Hg concentration (0.77 to 2253 ng/g), δ^{202}Hg (−2.59 to +0.85 ‰), and Δ^{199}Hg values (−0.29 to +0.21 ‰). Sulfides (pyrite, chalcopyrite and bornite) from the three Gangdese PCDs (Qulong, Jiama, and Zhibula) display δ^{202}Hg values ranging from −2.14 to +0.69 ‰ and Δ^{199}Hg from −0.15 to +0.10 ‰. Sulfides (pyrite) from Yulong PCD display a similar range in δ^{202}Hg (−2.59 to +0.85 ‰), but a larger range for Δ^{199}Hg values (−0.29 to +0.21 ‰). The juvenile lower crustal rocks from the Milin area display low Hg concentrations (0.12 to 2.67 ng/g), mainly positive δ^{202}Hg (−0.33 to +1.59 ‰) and negative Δ^{199}Hg values (−0.20 to +0.01 ‰). Ultrapotassic mafic rocks display low Hg levels (0.29 to 6.03 ng/g), negative δ^{202}Hg (−1.48 to −0.48 ‰) and mainly negative Δ^{199}Hg (−0.42 to +0.06 ‰). All samples show a positive correlation between Δ^{201}Hg and Δ^{199}Hg with the $\Delta^{199}\mathrm{Hg}/\Delta^{201}\mathrm{Hg} \approx 1$ ($R^2 = 0.68$) (Fig. 2b), consistent with that observed in the atmosphere-land-ocean system (Blum *et al.*, 2014). The LOI values of the juvenile lower crustal rocks and ultrapotassic mafic rocks are less than 3 wt. %, indicating that these samples are fresh and have not undergone significant weathering or alteration.

Discussion

The existence of terrestrial Hg in the lithospheric mantle and juvenile lower crust. Ultrapotassic mafic rocks and juvenile lower crustal rocks display low LOI values (<3 wt. %; Table S-3). A lack of correlation between the LOI and Hg concentrations, and δ^{202}Hg or Δ^{199}Hg values of these rocks (Fig. S-5) suggests that the variations of Hg abundance and isotopic composition do not correlate with alteration. Since magmatic processes trigger minor Hg-MDF but not Hg-MIF (Moynier *et al.*, 2021), we use Δ^{199}Hg instead of δ^{202}Hg to constrain the sources of Hg in the rock samples.

The primitive mantle displays low Hg concentrations (0.4–0.6 ng/g) and near-zero Δ^{199}Hg (0.00 ± 0.10 ‰; 2 s.d.) (Moynier *et al.*, 2021). The elevated Hg concentrations (1.79 ± 4.28 ng/g;

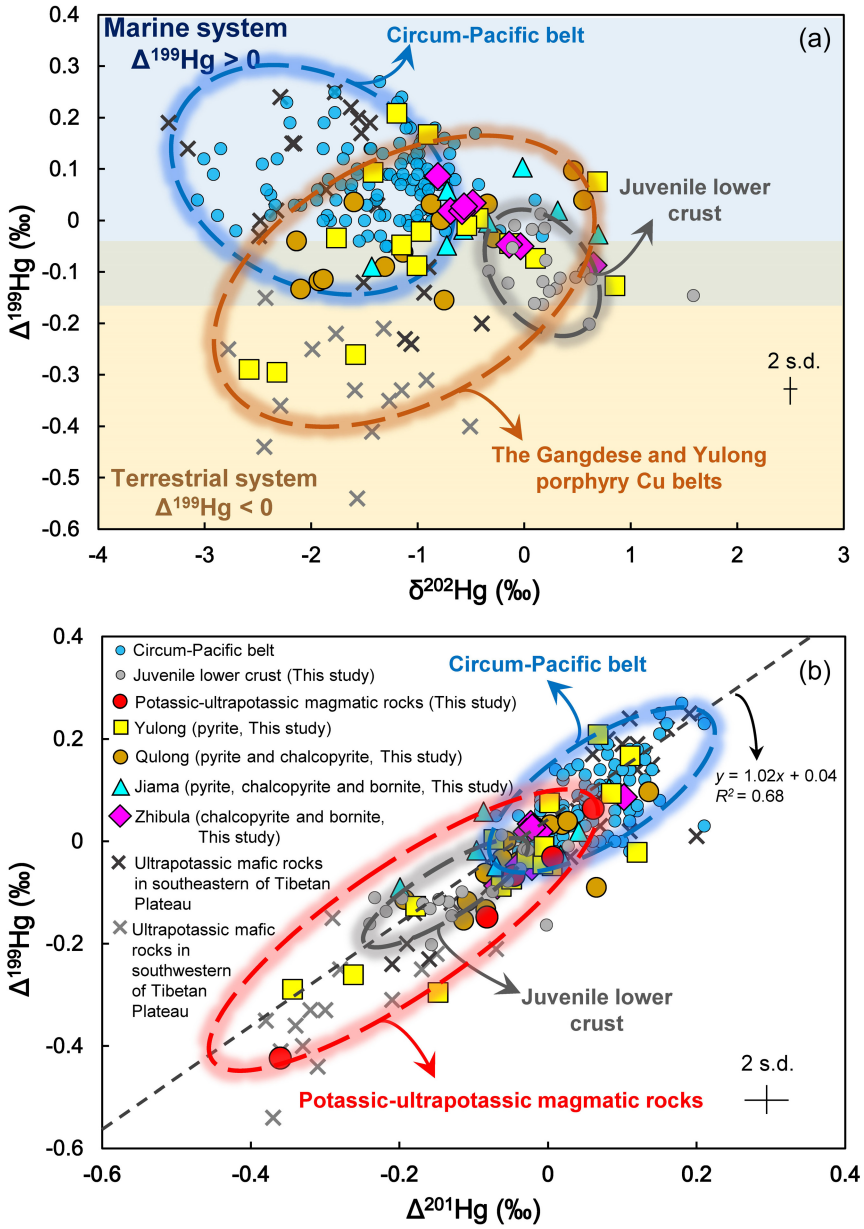

Figure 2 **(a)** Δ^{199}Hg *versus* δ^{202}Hg and **(b)** Δ^{199}Hg *versus* Δ^{201}Hg for the Gangdese and Yulong PCDs, juvenile lower crust rocks and potassic-ultrapotassic rocks in the Tibetan Plateau. Data sources: marine and terrestrial systems (Blum *et al.*, 2014); Circum-Pacific belt (Deng *et al.*, 2021; Gao *et al.*, 2024a); ultrapotassic mafic rocks in south Tibet (Xu *et al.*, 2024). s.d., standard deviation.

2 s.d., $n = 5$) and negative Δ^{199}Hg (−0.12 ± 0.33 ‰; 2 s.d., $n = 5$) values in ultrapotassic mafic rocks suggest the existence of recycled terrestrially derived Hg in their magma source, since Hg in terrestrial reservoirs displays negative Δ^{199}Hg values (Blum *et al.*, 2014). Measurements of Sr-Nd-Pb isotopes confirmed that these ultrapotassic mafic rocks were derived from the SCLM fertilised by terrestrial components *via* Indian Plate continental subduction (Wang *et al.*, 2020). Furthermore, Sr-Nd-Pb isotope data suggest that crustal material was incorporated early into the juvenile lower crust during the melting-assimilation-storage-homogenisation process (Miller *et al.*, 1999), which could explain the negative Δ^{199}Hg values in juvenile lower crustal rocks.

Genesis of PCDs in the Himalayan-Tibetan belt. Due to the chalcophile behaviour of Hg and the lack of Hg-MIF during metallogenic processes (Deng *et al.*, 2021), Δ^{199}Hg can be used to trace the source of Hg and other metals in PCDs. The Δ^{199}Hg signals of sulfides in Yulong and Gangdese PCDs show negative to positive Δ^{199}Hg values of −0.29 to +0.21 ‰. These values are different from the overall positive Δ^{199}Hg values for epithermal Au deposits (−0.03 to +0.27 ‰) and porphyry Mo deposits (−0.05 to +0.24 ‰) in the Circum-Pacific belt (Fig. 2), which receive Hg from subducted marine sediments (Deng *et al.*, 2021; Gao *et al.*, 2024a).

Potential metal sources for PCDs of the Himalayan-Tibetan orogenic belt include the juvenile lower crust and SCLM (Wang *et al.*, 2018; Xu *et al.*, 2023). In Figure 2, 17 sulfides from the Gangdese PCDs and 9 sulfides from the Yulong PCD display Δ^{199}Hg values within the range of juvenile lower crustal rocks, suggesting that they received large fractions of Hg from the juvenile lower crust. However, the non-zero Δ^{199}Hg values in other sulfides in these PCDs, either below −0.1 ‰ or above +0.1 ‰, suggest that the juvenile lower crust was not the sole source of Hg. Photoreduction of Hg(II) results in negative and

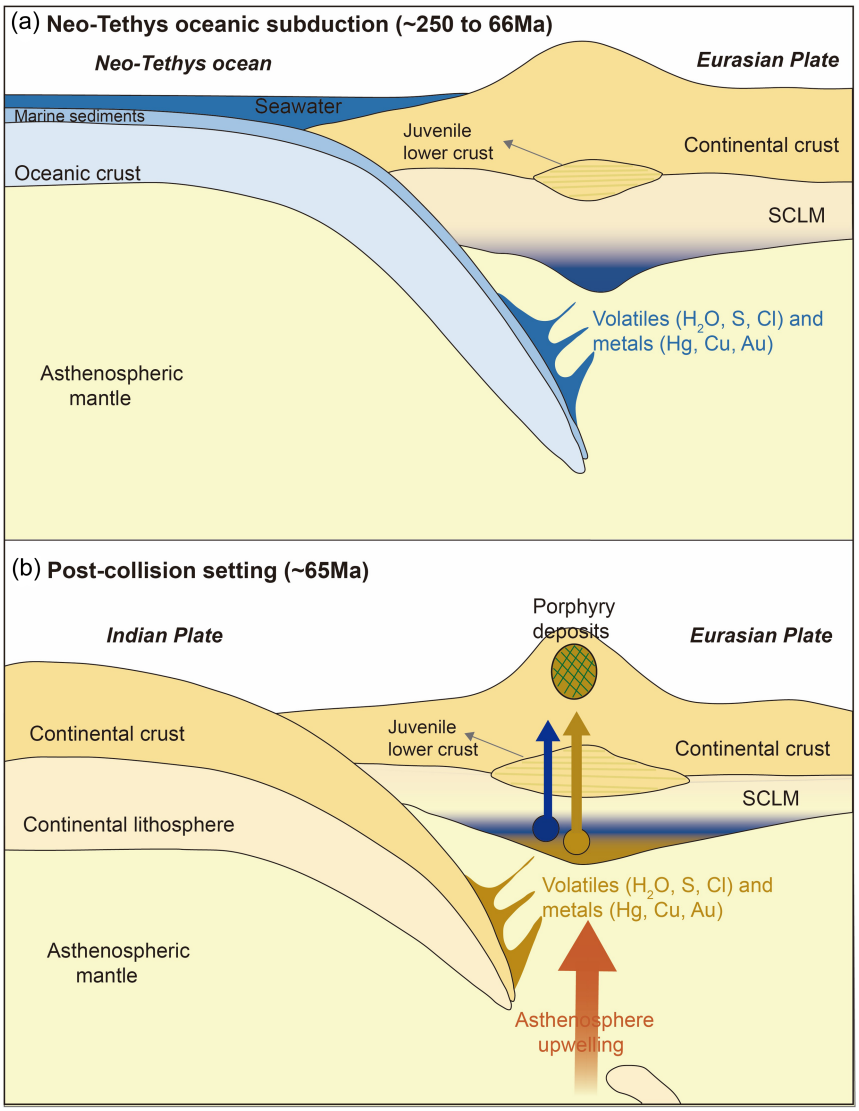

Figure 3 Genetic model of PCDs in the Alpine-Himalayan belt. **(a)** The Neo-Tethys oceanic subduction introduced large amounts of ocean-derived Hg released from subducted marine sediments into the SCLM. **(b)** Indian-Eurasia continental collision introduced terrestrially derived Hg into the SCLM, and tearing of the subducting Indian lithosphere triggered asthenospheric upwelling, leading to melting of the SCLM to generate large volumes of metal- and volatile-rich magma and magmatic-hydrothermal fluids.

positive Δ^{199}Hg values in terrestrial and marine systems, respectively (Blum *et al.*, 2014). Three sulfides (chalcopyrite, pyrite) display positive Δ^{199}Hg values above +0.1 ‰, and 8 sulfides (chalcopyrite, pyrite) display negative Δ^{199}Hg values below −0.1 ‰ (Fig. 2), suggesting the existence of recycled Hg from both marine and terrestrial systems. Since the Himalayan-Tibetan orogenic belt was influenced by the Neo-Tethys oceanic subduction followed by the Indian-Eurasian continental collision, the coexistence of positive and negative Δ^{199}Hg values in the Gangdese and Yulong PCDs may be a consequence of dual stage fertilisation of the SCLM.

The Neo-Tethys oceanic subduction may have fertilised the SCLM by marine-derived Hg released from subducted marine sediments (Fig. 3a), as supported by positive Δ^{199}Hg values of ultrapotassic mafic rocks (Xu *et al.*, 2024). The positive Δ^{199}Hg values above +0.1 ‰ in the studied Gangdese and Yulong PCDs confirm the contribution of recycled marine Hg released from the fertilised SCLM. Crustal assimilation, which produces S-type granites, may impart negative Δ^{199}Hg values to Gangdese and Yulong PCDs. However, the lack of coeval S-type melts in the eastern Gangdese area suggests limited crustal assimilation (Li *et al.*, 2022). The negative Δ^{199}Hg values of Gangdese and Yulong PCDs are more reasonably explained by the Indian-Eurasian continental collision, which fertilised the SCLM by introducing abundant terrestrially derived Hg (Fig. 3b), as supported by the negative Δ^{199}Hg values of ultrapotassic mafic rocks (Xu *et al.*, 2024). Following the dual stage fertilisation processes, the subducted Indian continental lithosphere underwent tearing, triggering upwelling of the asthenosphere, leading to melting of the metasomatised SCLM and juvenile lower crust, favouring the formation of large volumes of metal- and volatile-rich magma and an associated large number of PCDs (Hou *et al.*, 2015; Zheng *et al.*, 2019; Xu *et al.*, 2024).

Conclusions

The formation of massive PCDs in the Tibetan Plateau is to be expected. Based on Hg isotopes, this study demonstrates that the Neo-Tethys oceanic subduction and Indian-Eurasia continental collision have extensively fertilised the SCLM beneath the Tibetan Plateau. These two processes transported

large amounts of metals and volatiles from recycled terrestrial and marine sediments to the SCLM, providing a material base for the metallogeny of PCDs. This study highlights the powerful use of Hg isotopes in tracing recycled metals and volatiles in the mantle, and highlights the crucial role of multistage plate subduction and mantle fertilisation in the generation of PCDs in the Himalayan-Tibetan orogenic belt.

Acknowledgements

This work is supported by the Hundred Talent Plan through the Chinese Academy of Sciences. We thank Rui Wang for providing some of the samples, Massimo Chiaradia for his assistance in data interpretation, and Manuel Keith and an anonymous reviewer for providing valuable comments.

Editor: Raul O.C. Fonseca

Additional Information

Supplementary Information accompanies this letter at https://www.geochemicalperspectivesletters.org/article2519.

Cite this letter as: Wang, X., Gao, L., Bai, Z., Huang, M., Zhu, J., Yin, R. (2025) Large Cu endowment in the Tibetan Plateau as a result of dual stage mantle fertilisation. *Geochem. Persp. Let.* 35, 24–30. https://doi.org/10.7185/geochemlet.2519

References

Blum, J.D., Bergquist, B.A. (2007) Reporting of variations in the natural isotopic composition of mercury. *Analytical and Bioanalytical Chemistry* 388, 353–359. https://doi.org/10.1007/s00216-007-1236-9

Blum, J.D., Sherman, L.S., Johnson, M.W. (2014) Mercury Isotopes in Earth and Environmental Sciences. *Annual Review of Earth and Planetary Sciences* 42, 249–269. https://doi.org/10.1146/annurev-earth-050212-124107

Deng, C., Sun, G., Rong, Y., Sun, R., Sun, D., Lehmann, B., Yin, R. (2021) Recycling of mercury from the atmosphere-ocean system into volcanic-arc–associated epithermal gold systems. *Geology* 49, 309–313. https://doi.org/10.1130/G48132.1

Gao, L., Sun, D., Tian, Z., Luo, A., Lehmann, B., Yin, R. (2024a) Positive Δ^{199}Hg anomalies in Mesozoic porphyry Mo deposits of Northeastern China and their implications to the metallogeny of arc-related hydrothermal systems at convergent margins. *Chemical Geology* 645, 121880. https://doi.org/10.1016/j.chemgeo.2023.121880

Gao, L., Sun, D., Wang, X., Chen, D., Tian, Z., Luo, A., Yin, R. (2024b) A Catalyst Tube-Equipped Dual-Stage Tube Furnace System for Accurate Hg Isotopic Determination of Ore Samples Using Neptune Plus Multicollector Inductively Coupled Plasma Mass Spectrometry. *Analytical Chemistry* 96, 17560–17566. https://doi.org/10.1021/acs.analchem.4c03041

Hou, Z., Zhang, H., Pan, X., Yang, Z. (2011) Porphyry Cu (–Mo–Au) deposits related to melting of thickened mafic lower crust: Examples from the eastern Tethyan metallogenic domain. *Ore Geology Reviews* 39, 21–45. https://doi.org/10.1016/j.oregeorev.2010.09.002

Hou, Z., Yang, Z., Lu, Y., Kemp, A., Zheng, Y., Li, Q., Tang, J., Yang, Z., Duan, L. (2015) A genetic linkage between subduction- and collision-related porphyry Cu deposits in continental collision zones. *Geology* 43, 247–250. https://doi.org/10.1130/G36362.1

Hou, Z., Yang, Z., Wang, R., Zheng, Y. (2020) Further discussion on porphyry Cu-Mo-Au deposit formation in mainland China. *Earth Science Frontiers* 27, 20–44. https://doi.org/10.13745/j.esf.sf.2020.3.8

Li, J.-X., Qin, K.-Z., Li, G.-M., Xiao, B., Chen, L., Zhao, J.-X. (2011) Post-collisional ore-bearing adakitic porphyries from Gangdese porphyry copper belt, southern Tibet: Melting of thickened juvenile arc lower crust. *Lithos* 126, 265–277. https://doi.org/10.1016/j.lithos.2011.07.018

Li, W.-T., Ding, H.-X., Zhang, Z.-M., Larson, K.P. (2022) Petrogenesis of metasedimentary rocks in the deep crust of the eastern Gangdese arc. *Lithos* 430–431, 106884. https://doi.org/10.1016/j.lithos.2022.106884

Liang, H.-Y., Campbell, I.H., Allen, C., Sun, W.-D., Liu, C.-Q., Yu, H.-X., Xie, Y.-W., Zhang, Y.-Q. (2006) Zircon Ce^{4+}/Ce^{3+} ratios and ages for Yulong ore-bearing porphyries in eastern Tibet. *Mineralium Deposita* 41, 152–159. https://doi.org/10.1007/s00126-005-0047-1

Metcalfe, I. (2021) Multiple Tethyan ocean basins and orogenic belts in Asia. *Gondwana Research* 100, 87–130. https://doi.org/10.1016/j.gr.2021.01.012

Miller, C., Schuster, R., Klötzli, U., Frank, W., Purtscheller, F. (1999) Post-Collisional Potassic and Ultrapotassic Magmatism in SW Tibet: Geochemical and Sr–Nd–Pb–O Isotopic Constraints for Mantle Source Characteristics and Petrogenesis. *Journal of Petrology* 40, 1399–1424. https://doi.org/10.1093/petroj/40.9.1399

Moynier, F., Jackson, M.G., Zhang, K., Cai, H., Halldórsson, S.A., Pik, R., Day, J.M.D., Chen, J. (2021) The Mercury Isotopic Composition of Earth's Mantle and the Use of Mass Independently Fractionated Hg to Test for Recycled Crust. *Geophysical Research Letters* 48, e2021GL094301. https://doi.org/10.1029/2021GL094301

Richards, J.P. (2009) Postsubduction porphyry Cu-Au and epithermal Au deposits: Products of remelting of subduction-modified lithosphere. *Geology* 37, 247–250. https://doi.org/10.1130/G25451A.1

Sillitoe, R.H. (2010) Porphyry Copper Systems. *Economic Geology* 105, 3–41. https://doi.org/10.2113/gsecongeo.105.1.3

Sun, J.-L., Bai, Z.-J., Zhong, H., Liu, X., Zhu, J.-J., Chen, L., Zhu, W.-G. (2024) Sulfide saturation in reduced magmas during generation of the Gangdese juvenile lower crust: Implications for porphyry Cu–Au mineralization in the Gangdese belt, Tibet. *Mineralium Deposita* 59, 1387–1405. https://doi.org/10.1007/s00126-024-01269-0

Wang, P., Zhao, G., Han, Y., Liu, Q., Zhou, N., Yao, J., Li, J., Li, Y. (2020) Post-collisional potassic rocks in Western Kunlun, NW Tibet Plateau: Insights into lateral variations in the crust-mantle structure beneath the India-Asia collision zone. *Lithos* 370–371, 105645. https://doi.org/10.1016/j.lithos.2020.105645

Wang, R., Weinberg, R.F., Collins, W.J., Richards, J.P., Zhu, D.-c. (2018) Origin of postcollisional magmas and formation of porphyry Cu deposits in southern Tibet. *Earth-Science Reviews* 181, 122–143. https://doi.org/10.1016/j.earscirev.2018.02.019

Wilkinson, J.J. (2013) Triggers for the formation of porphyry ore deposits in magmatic arcs. *Nature Geoscience* 6, 917–925. https://doi.org/10.1038/ngeo1940

Xu, B., Yin, R.-S., Chiaradia, M., Miao, Z., Griffin, W.L., Hou, Z.-Q., Yang, Z.-M., O'Reilly, S.Y. (2024) Mercury isotope evidence for the importance of recycled fluids in collisional ore systems. *Science Advances* 10, eadp7383. https://doi.org/10.1126/sciadv.adp7383

Xu, L., Bi, X., Hu, R., Qi, Y., Tang, Y., Wang, X., Zhu, J. (2016) Redox states and genesis of magmas associated with intra-continental porphyry Cu–Au mineralization within the Jinshajiang–Red River alkaline igneous belt, SW China. *Ore Geology Reviews* 73, 330–345. https://doi.org/10.1016/j.oregeorev.2015.05.007

Xu, L.-L., Zhu, J.-J., Huang, M.-L., Pan, L.-C., Hu, R., Bi, X.-W. (2023) Genesis of hydrous-oxidized parental magmas for porphyry Cu (Mo, Au) deposits in a postcollisional setting: examples from the Sanjiang region, SW China. *Mineralium Deposita* 58, 161–196. https://doi.org/10.1007/s00126-022-01143-x

Yang, Z., Cooke, D.R. (2019) Porphyry Copper Deposits in China. In: Chang, Z., Goldfarb, R.J. (Eds.) *Mineral Deposits of China*. Society of Economic Geologists, Littleton, 133–187. https://doi.org/10.5382/SP.22.05

Yin, R., Krabbenhoft, D.P., Bergquist, B.A., Zheng, W., Lepak, R.F., Hurley, J.P. (2016) Effects of mercury and thallium concentrations on high precision determination of mercury isotopic composition by Neptune Plus multiple collector inductively coupled plasma mass spectrometry. *Journal of Analytical Atomic Spectrometry* 31, 2060–2068. https://doi.org/10.1039/C6JA00107F

Yin, R., Chen, D., Pan, X., Deng, C., Chen, L., Song, X., Yu, S., Zhu, C., Wei, X., Xu, Y., Feng, X., Blum, J.D., Lehmann, B. (2022) Mantle Hg isotopic heterogeneity and evidence of oceanic Hg recycling into the mantle. *Nature Communications* 13, 948. https://doi.org/10.1038/s41467-022-28577-1

Yin, R., Wang, X., Sun, R., Gao, L., Deng, C., Tian, Z., Luo, A., Lehmann, B. (2024) Linking the mercury biogeochemical cycle to the deep mercury cycle: A mercury isotope perspective. *Chemical Geology* 654, 122063. https://doi.org/10.1016/j.chemgeo.2024.122063

Zerkle, A.L., Yin, R., Chen, C., Li, X., Izon, G.J., Grasby, S.E. (2020) Anomalous fractionation of mercury isotopes in the Late Archean atmosphere. *Nature Communications* 11, 1709. https://doi.org/10.1038/s41467-020-15495-3

Zheng, Y.-C., Liu, S.-A., Wu, C.-D., Griffin, W.L., Li, Z.-Q., Xu, B., Yang, Z.-M., Hou, Z.-Q., O'Reilly, S.Y. (2019) Cu isotopes reveal initial Cu enrichment in sources of giant porphyry deposits in a collisional setting. *Geology* 47, 135–138. https://doi.org/10.1130/G45362.1

Zheng, Y.-C., Shen, Y., Wang, L., Griffin, W.L., Hou, Z.-Q. (2021) Collision-related porphyry Cu deposits formed by input of ultrapotassic melts into the sulfide-rich lower crust. *Terra Nova* 33, 582–589. https://doi.org/10.1111/ter.12550